Electronic Supplementary Information for

Large-scalable, ultrastable thin films for electromagnetic interference shielding

Jae Seo Park,[a‡] Ji Yong Park,[a‡] Kyunbae Lee,[b] Young Shik Cho,[c] Hyunji Shin,[a] Yeonsu Jung,[b] Chong Rae Park,[c] Taehoon Kim,[b*] Jae Ho Kim,[a,c,*] Seung Jae Yang[a,*]

[1]Department of Chemistry and Chemical Engineering, Education and Research Center for Smart Energy and Materials, Inha University, Incheon 22212, Republic of Korea

[2]Composites Research Division, Korea Institute of Materials Science (KIMS), Changwon 51508, Republic of Korea.

[3]Department of Materials Science and Engineering, Seoul National University, Seoul 08826, Republic of Korea

Corresponding authors: sjyang@inha.ac.kr (S. J. Yang), advho@snu.ac.kr (J. H. Kim), tkim67@kims.re.kr (T. Kim)

‡These authors contributed equally.

Experimental section

Fabrication of DWNTF

The DWNT-aerogel was synthesized by floating catalyst chemical vapor deposition (FCCVD) process with a furnace temperature of 1200 °C. Before the synthesis, the carrier gases (H_2, 99.999 % and Ar, 99.999 %) were supplied to a vertical-type tube furnace to compose continuous flow. Subsequently, the feedstock that consisted of a catalyst, promoter, and carbon source was fed into the furnace. Ferrocene (Sigma Aldrich, 98%), thiophene (Sigma Aldrich, 99%), and methane (99.999 %) were used as the catalyst, promoter, and carbon source, respectively. At the outlet of the tube furnace, the as-synthesized DWNT-aerogel layer was collected into the surface of PTFE film using the guide roller at a constant rotation speed, resulting in the formation of DWNTF.

Hybridization of cMOF with DWNTF

Before hybridization, the DWNTFs were washed and densified by ethanol. Cobalt nitrate hexahydrate (1.175 g, Sigma Aldrich, 98%) and hexahydroxytriphenylene (0.650 g, TCI Chemicals, 95%) were dissolved in 500 ml of distilled water/N,N-dimethylformamide (DMF, Daejung, 99.5%) (v/v = 1:1) mixed solution. Subsequently, the 20 × 10 cm DWNTF on the PTFE film was immersed into the prepared solution and heated at 85 ℃ for 18 hours to synthesize cMOF@DWNTF, resulting in a dark brown color solution. The reacted solution was cooled naturally to room temperature under an ambient atmosphere. The cMOF@DWNTF was washed first with distilled water (three times, 500 ml) and then with ethanol (three times, 500 ml). Subsequently, cMOF@DWNTF was vacuum-dried at 120 ℃ overnight to remove the residual solvents.

Synthesis of independent cMOF film

Cobalt nitrate hexahydrate (0.235 g, Sigma Aldrich, 98%) and hexahydroxytriphenylene (0.130 g, TCI Chemicals, 95%) were dissolved in 100 ml of distilled water/N,N-dimethylformamide (DMF, Daejung, 99.5%) (v/v = 1:1) mixed solution. Subsequently, the prepared mixture was heated up to 85 °C for 18 hours at convection oven. After that, the as-formed thin-film at the air/liquid interface was transferred into glass substrate, and dried under vacuum at 120 ℃ overnight for the further characterization.

Synthesis of other types of cMOF@DWNTF

DWNTF with 60 aerogel layers, Ni- and Cu-based cMOFs@DWNTFs were synthesized by the same procedure with Co-based cMOF@DWNTF using nickel nitrate hexahydrate (1.173 g, Sigma Aldrich, 98%) and copper nitrate trihydrate (0.976, Sigma Aldrich, 98%) as metal precursors, respectively.

Materials characterizations

The morphologies of the materials were investigated by scanning electron microscopy (SEM, SU8010, Hitachi). The physicochemical structure was analyzed by Raman spectroscopy (Ramantouch, Nanophoton) with a laser wavelength of 532 nm. The microstructures were studied by transmission electron microscopy (TEM, JEM-2100F and JEM-F200, JEOL) with an accelerating voltage of 200 kV. Analysis of the bonding state was carried out by X-ray photoelectron spectroscopy (XPS, K-Alpha, Thermo Fisher) using Al Kα radiation. Thermogravimetric analysis (TGA, TGA N1000, scinco) was conducted in an air atmosphere

using a thermo-program between 25 and 900 °C with a heating rate of 10 °C/min. The nitrogen adsorption–desorption isotherms (at 77 K) up to 1 bar were measured using a static volumetric gas adsorption instrument (Tri-Star II, Micromeritics). The crystal structure was investigated by X-ray diffraction (XRD, X'Pert-PRO. MRD) using Cu Kα radiation (λ = 1.54 Å). The optical transmittance was characterized by UV-Vis spectrophotometry (Evolution 201, Thermo Scientific) at 550 nm. Atomic force microscopy (AFM, Nanoscope Multimode IVa, Bruker) was employed to estimate the thickness of film-type materials. Tensile performances were investigated using a universal testing machine (UTM; RB 302 ML, R&B) at gage length of 10 mm and loading rate of 2 mm/min. The areal density of samples was quantified by an average weight per specific area with the highly precise balance (MS105DU, Mettler Toledo, 0.01 mg of resolution). For the reliability of estimation, DWNTF and cMOF@DWNTF with a sufficient area of 60 cm^2 were used, and the average of 10 weight records was divided by the area for calculation (Table S3). The sheet resistance was measured using a four-point probe station (M4P 205-System, MSTECH) with a source meter (2634B, Keithley). From the recorded sheet resistance, the following equation was used to determine the electrical conductivity of the samples:

$$\sigma = (R_s t)^{-1}$$

where σ is the electrical conductivity [S cm^{-1}], R_s is the sheet resistance [Ω sq^{-1}], and t is the thickness of samples [cm].

Shielding effectiveness measurements

The shielding effectiveness of the cMOF@DWNTF and DWNTF was examined using a vector network analyzer (Keysight N5222B) integrated with a WR-42 waveguide and a WR-90

waveguide over the frequency range of the K-band (18 – 26.5 GHz) and X-band (8.2 – 12.4 GHz), respectively. The shielding effectiveness, including the total shielding effectiveness (SE_T), the absorption effectiveness (SE_A), and reflection effectiveness (SE_R), was calculated from the measured scattering parameters based on the following equations:[8]

$$R = |S_{11}|^2 \quad (1)$$

$$T = |S_{21}|^2 \quad (2)$$

$$A = 1 - R - T \quad (3)$$

$$SE_R = 10log(\frac{1}{1-R}) \quad (4)$$

$$SE_A = -10log(\frac{T}{1-R}) \quad (5)$$

$$SE_T = SE_R + SE_A \quad (6)$$

where S_{11} and S_{21} are the scattering parameters; R is the reflectance; T is transmittance; A is absorbance.

Durability test to harsh conditions

cMOF@DWNTF was soaked into artificial seawater (3 wt.% of NaCl aqueous solution) for 12 hours to ensure structural stability. cMOF@DWNTF was rinsed with distilled water and ethanol before being vacuum-dried overnight at 120 ℃. For a demonstration of thermal stability, cMOF@DWNTF was placed in a convection oven set to 150 and 250 °C for 12 hours, respectively. For testing the mechanical stability, cMOF@DWNTF was repeatedly folded at a bending angle of 90° using the designed automatic bending machine.

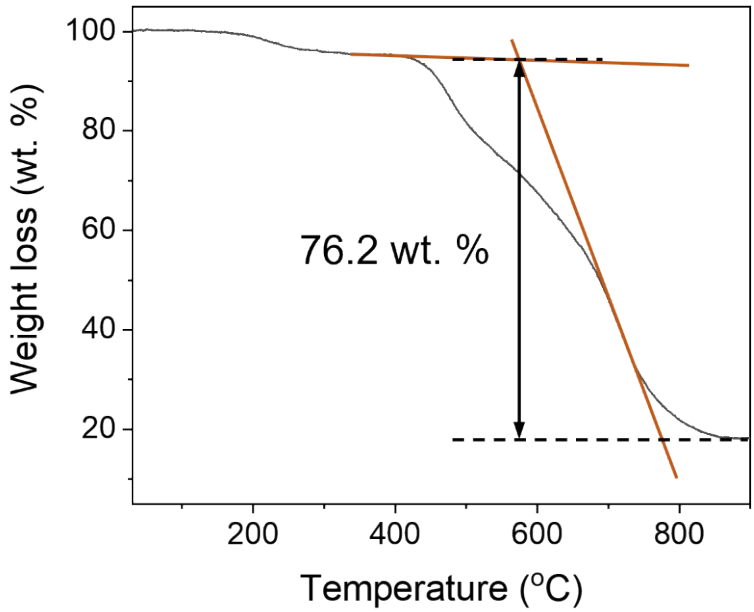

Fig. S1. TGA curve of the DWNTF under air atmosphere.

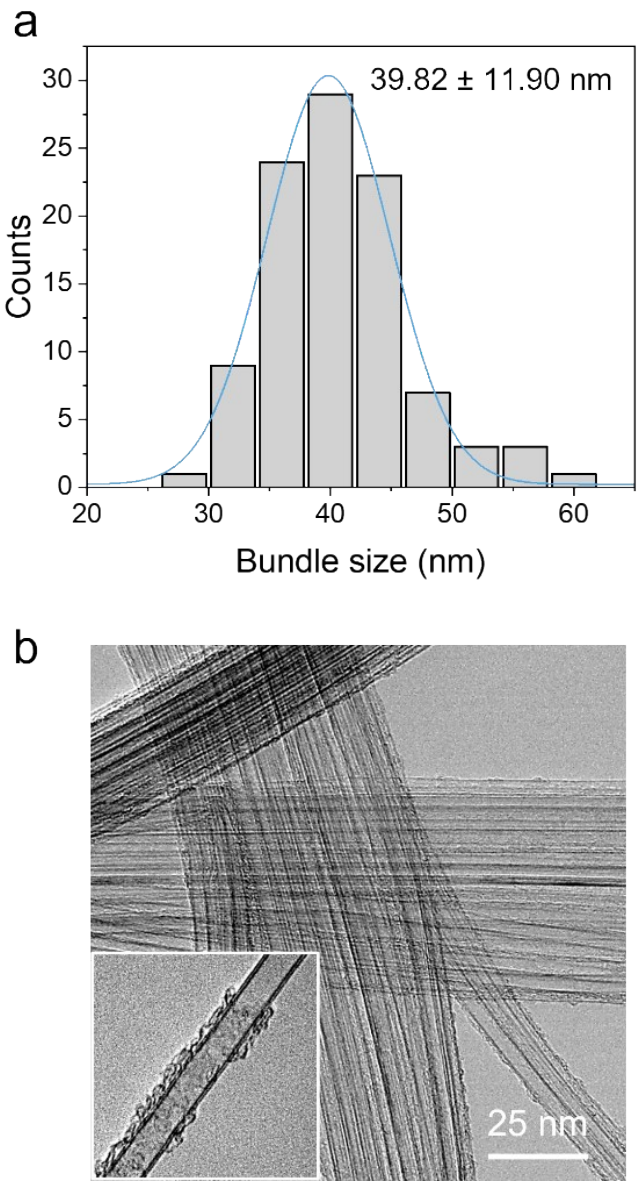

Fig. S2. a) Distribution of DWNT diameter estimated from SEM images and b) TEM image of as-synthesized DWNT bundle (inset: TEM image of individual DWNT).

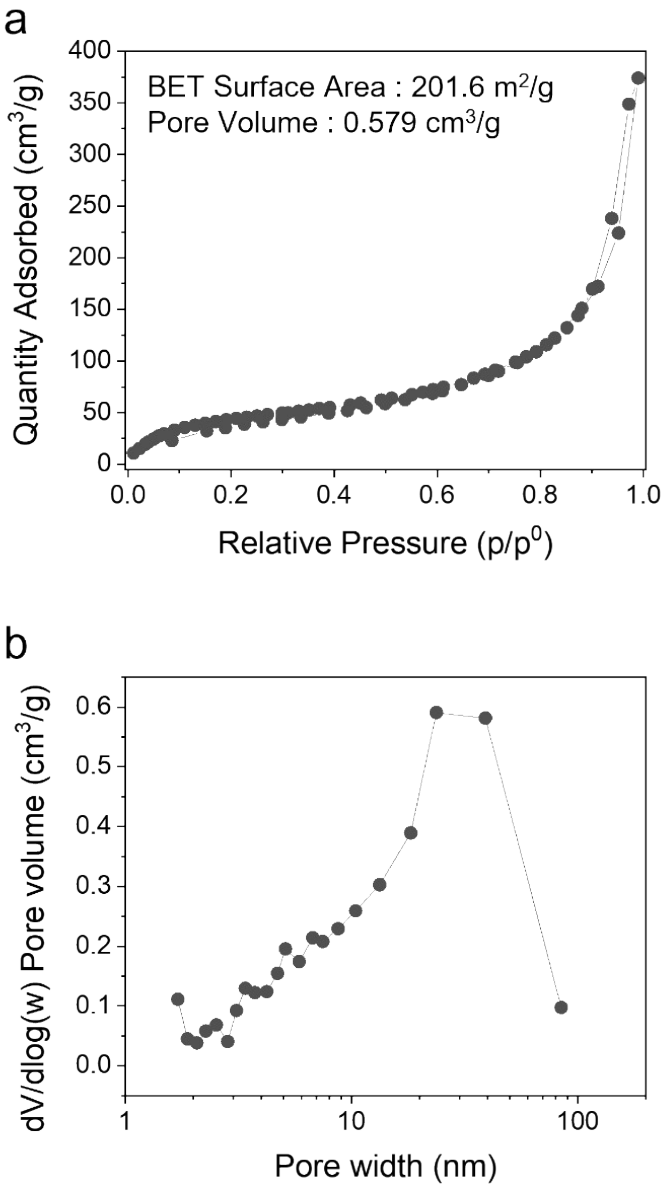

Fig. S3. (a) N_2 isotherms and (b) pore size distribution of DWNT aerogel.

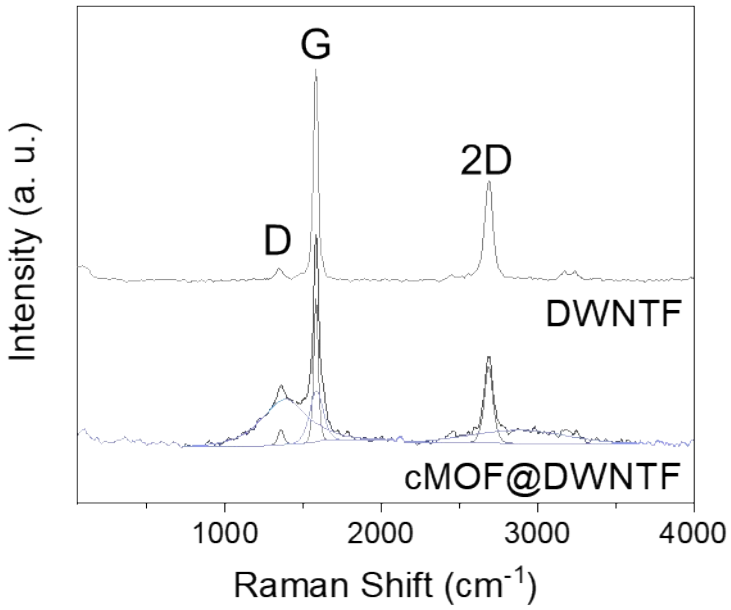

Fig. S4. Raman spectrum of the DWNTF and cMOF@DWNTF.

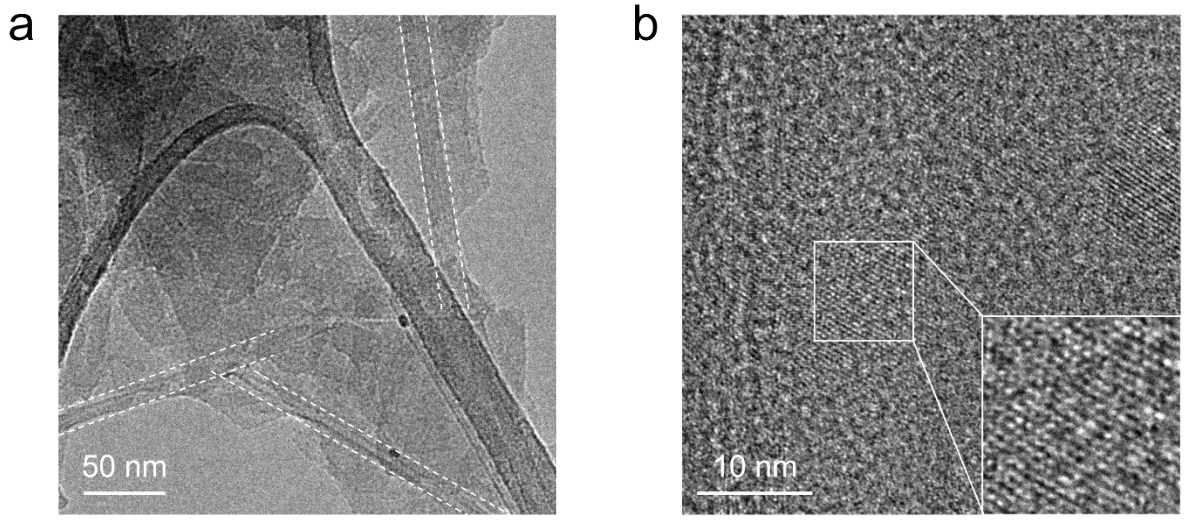

Fig. S5. a) and b) Additional TEM images of cMOF@DWNTF (White dashed line shows the presence of DWNT).

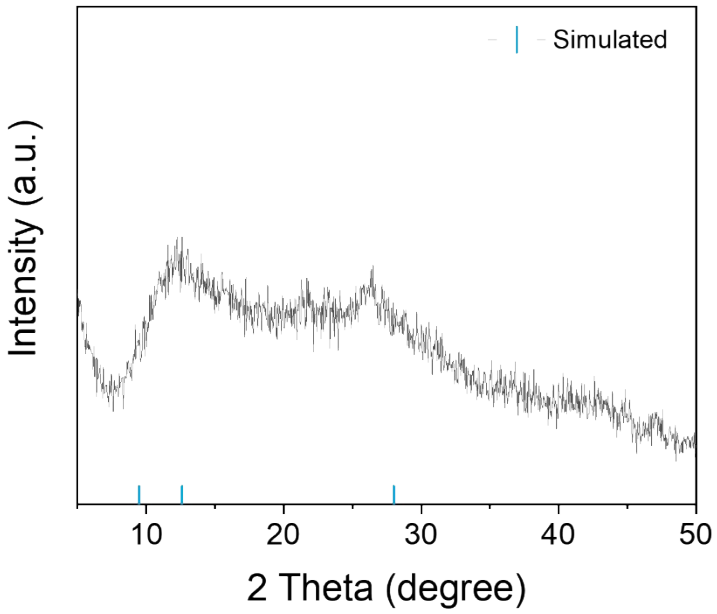

Fig. S6. XRD pattern of cMOF@DWNTF.

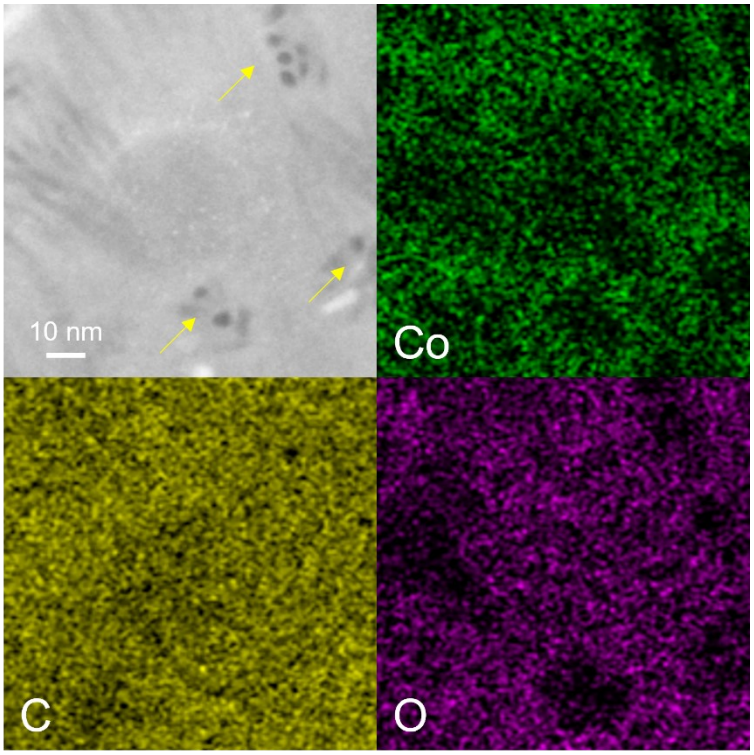

Fig. S7. TEM cross-sectional images and the results of EDS mapping of cMOF@DWNTF (Yellow arrows indicate the existence of DWNT bundles).

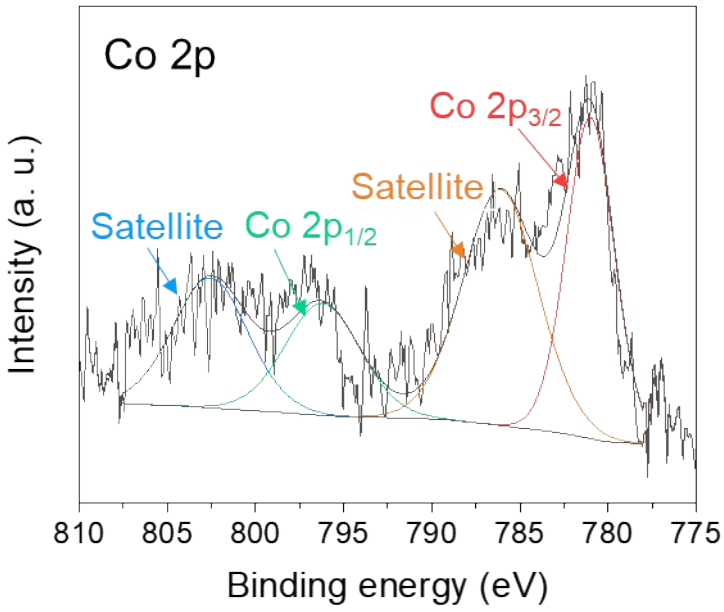

Fig. S8. XPS Co 2p spectra of cMOF@DWNTF.

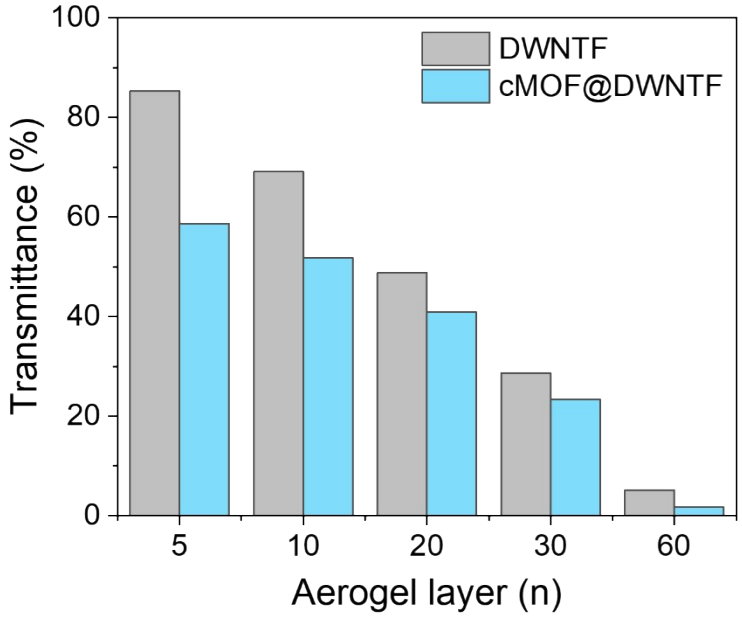

Fig. S9. Optical transmittance of DWNTF and cMOF@DWNTF with different aerogel layers.

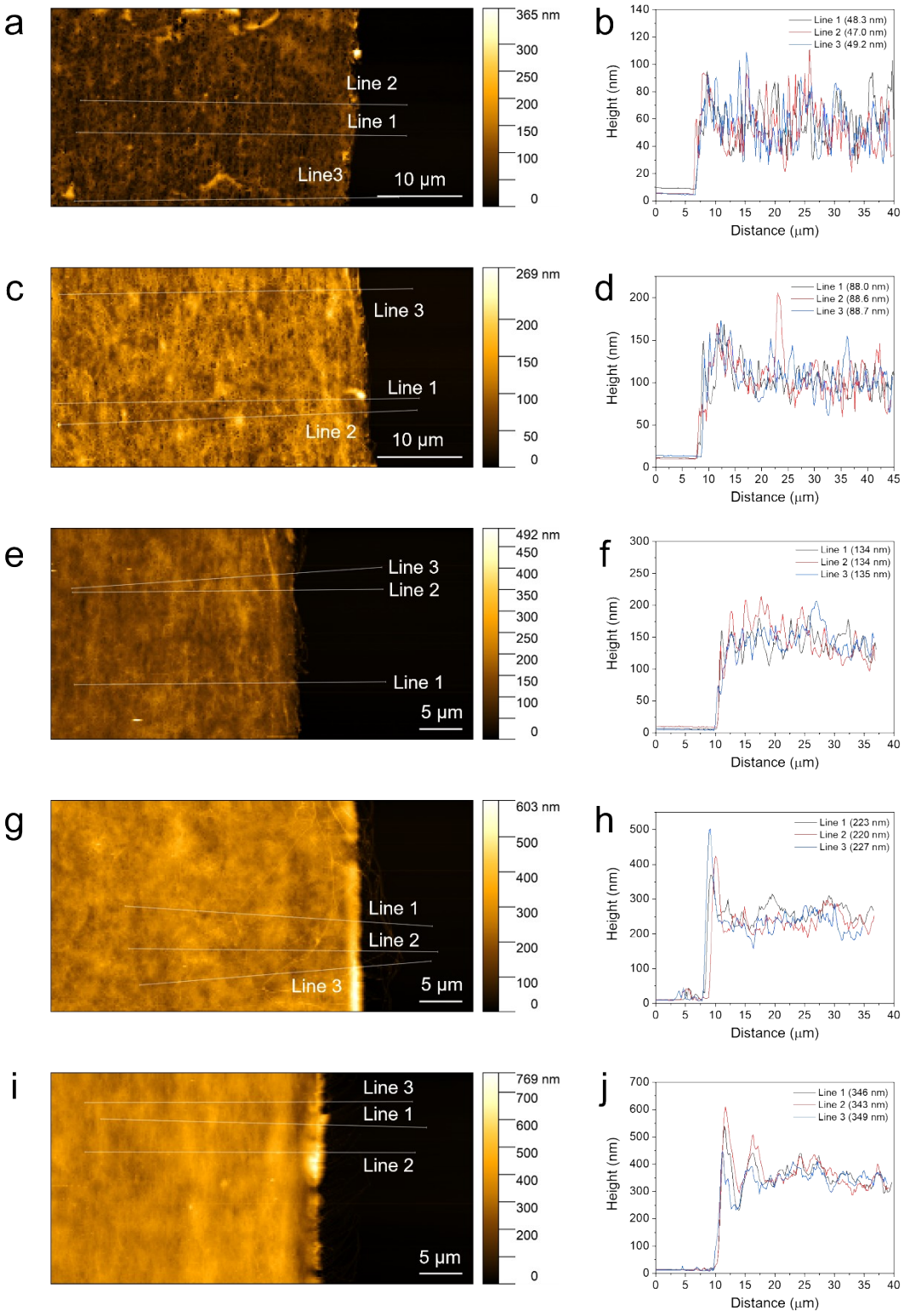

Fig. S10. AFM images and height profiles for the thickness measurement of DWNTF with a) and b) five layers, c) and d) 10 layers, e) and f) 20 layers, g) and h) 30 layers and i) and j) 60 layers.

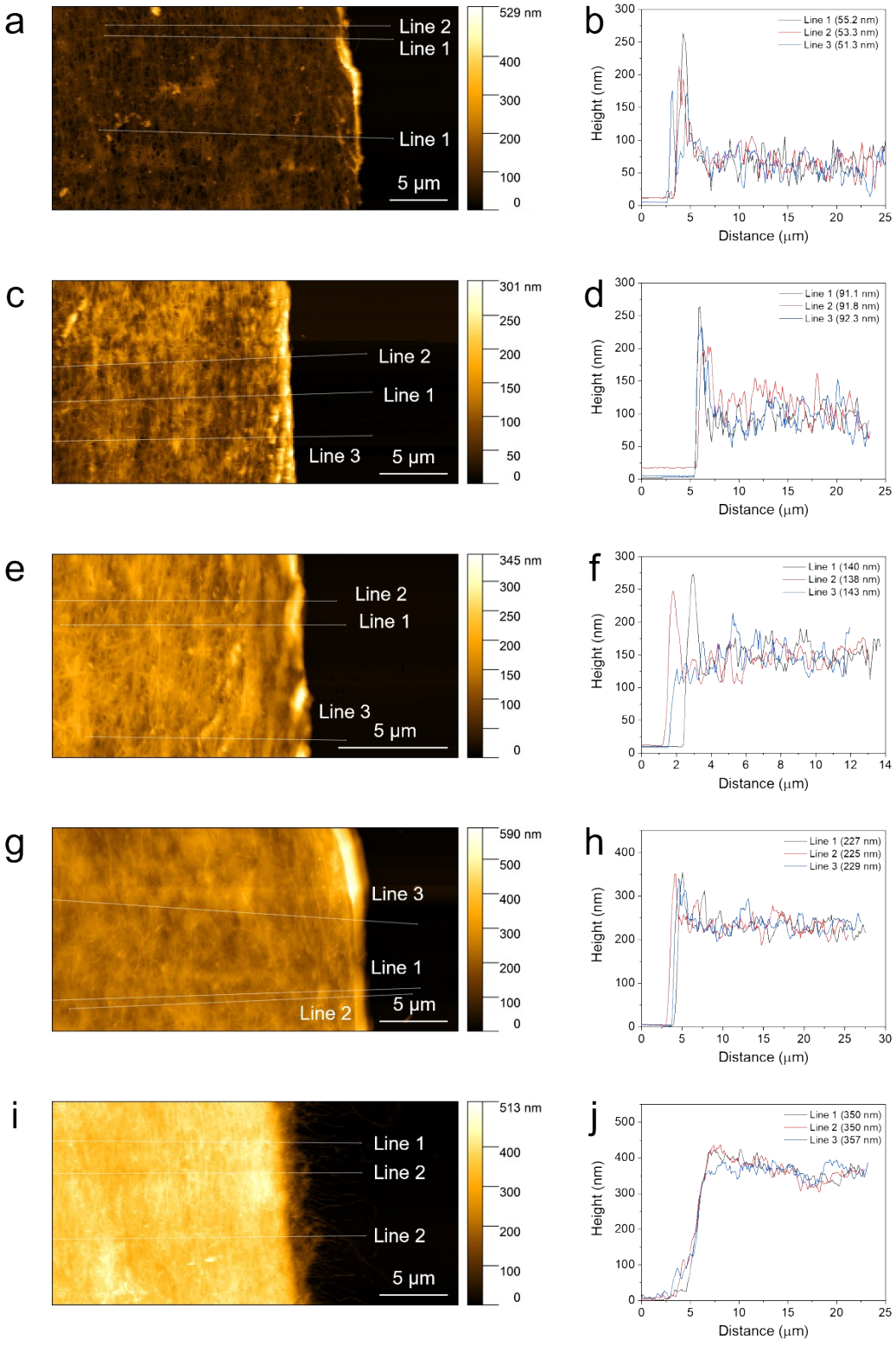

Fig. S11. AFM images and height profiles for the thickness measurement of cMOF@DWNTF with a) and b) five layers, c) and d) 10 layers, e) and f) 20 layers, g) and h) 30 layers, and i) and j) 60 layers.

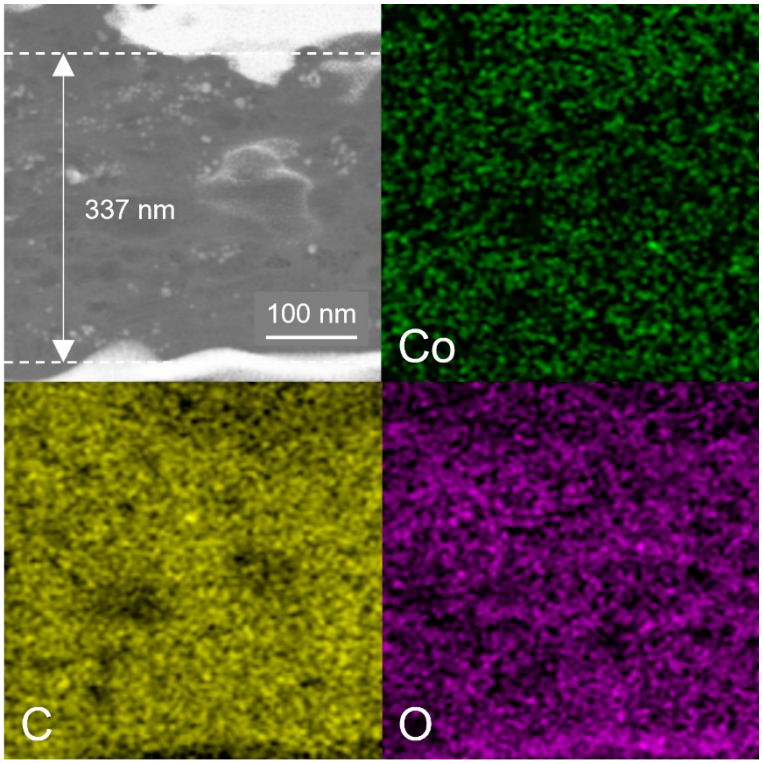

Fig. S12. SEM cross-sectional image and EDS elemental mapping of cMOF@DWNTF with 60 aerogel layers.

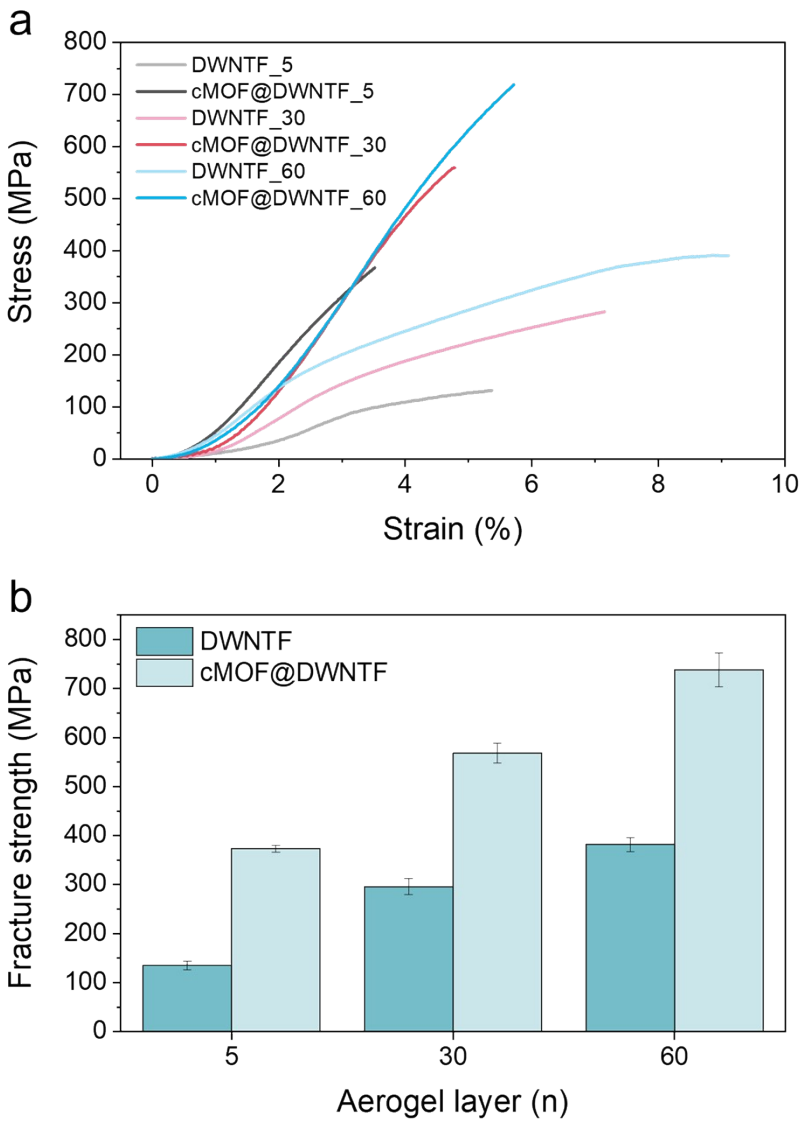

Fig. S13. (a) Stress-strain curves and (b) fracture strength of DWNTF and cMOF@DWNTF with different numbers of aerogel layers.

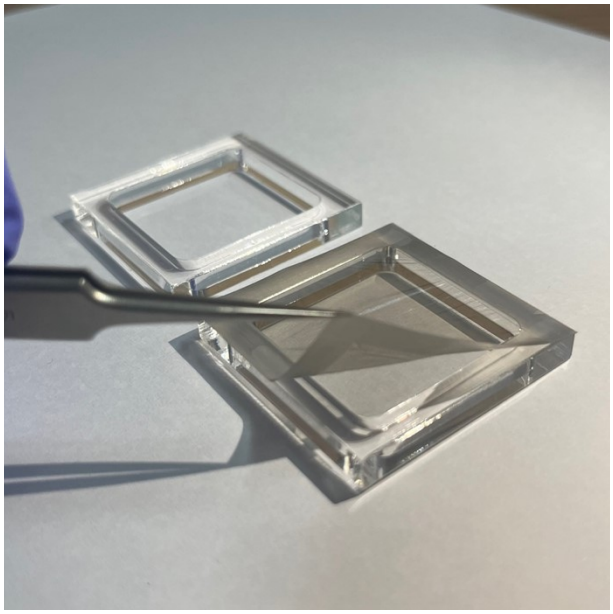

Fig. S14. Digital images of empty acrylic frame and cMOF@DWNTF with five aerogel layers placed on the frame.

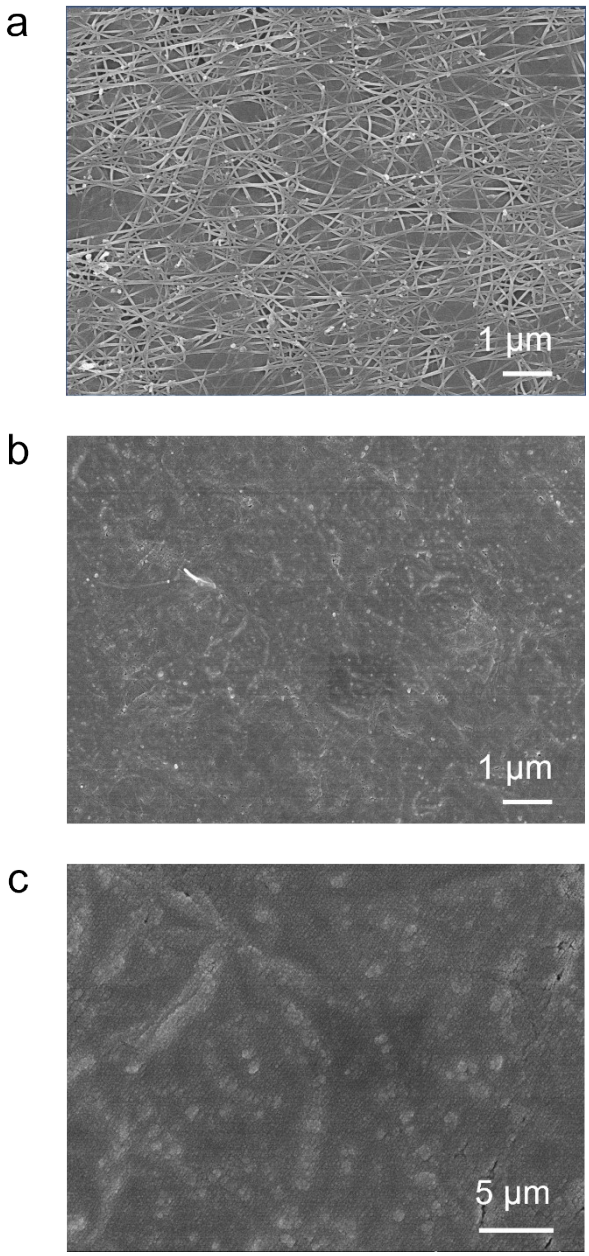

Fig. S15. SEM images of a) DWNTF and b) and c) cMOF@DWNTF with five aerogel layers.

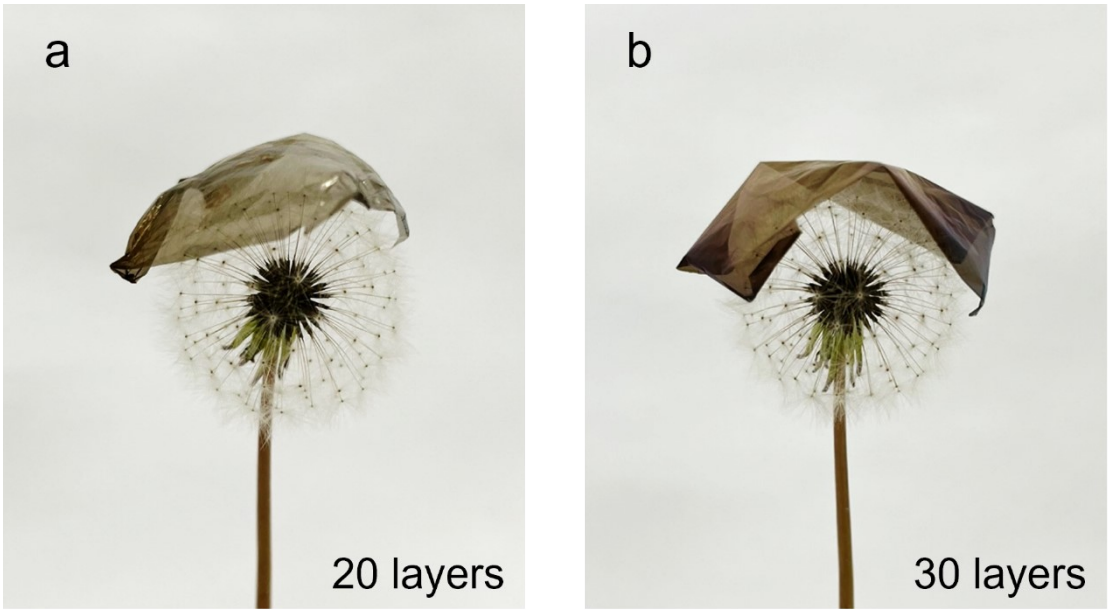

Fig. S16. a) and b) cMOF@DWNTF with different aerogel layers placed on a dandelion seed.

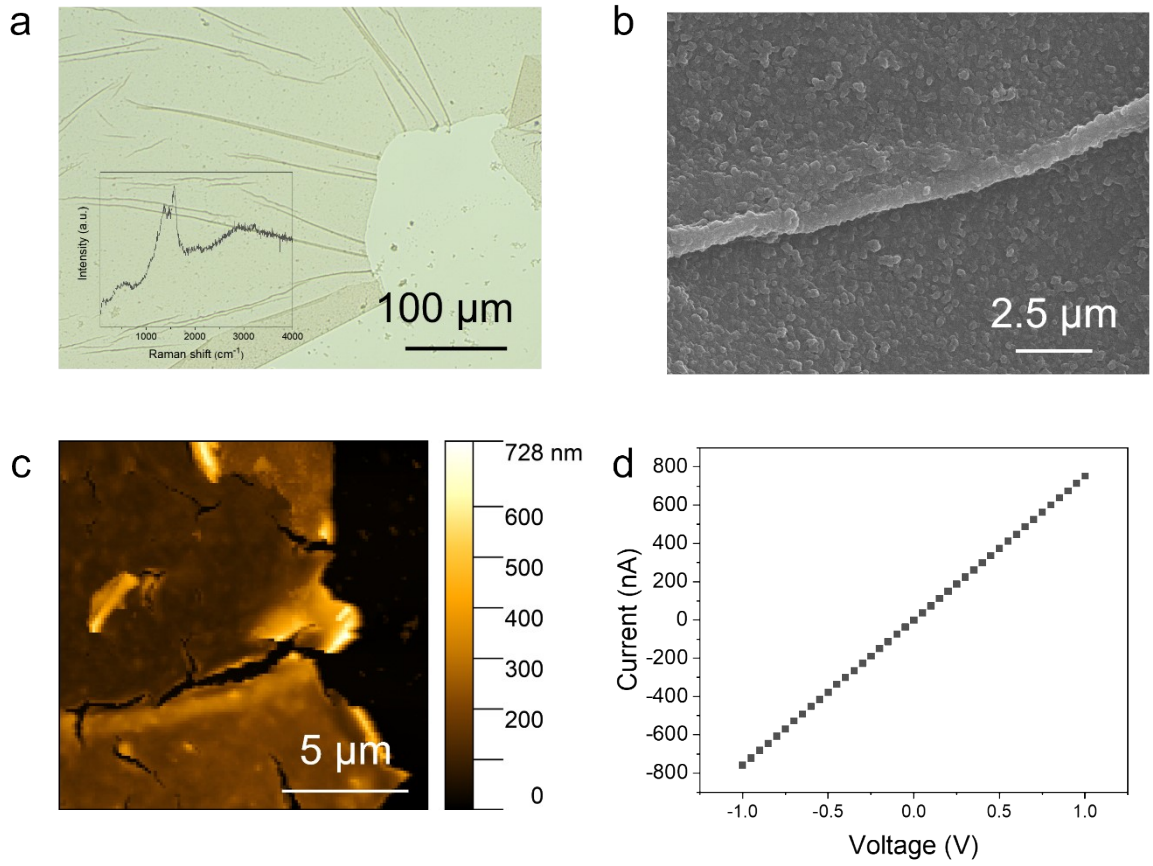

Fig. S17. a) Optical image (inset: Raman spectrum), b) SEM image, c) AFM image, and d) current versus voltage curve of the independent cMOF film.

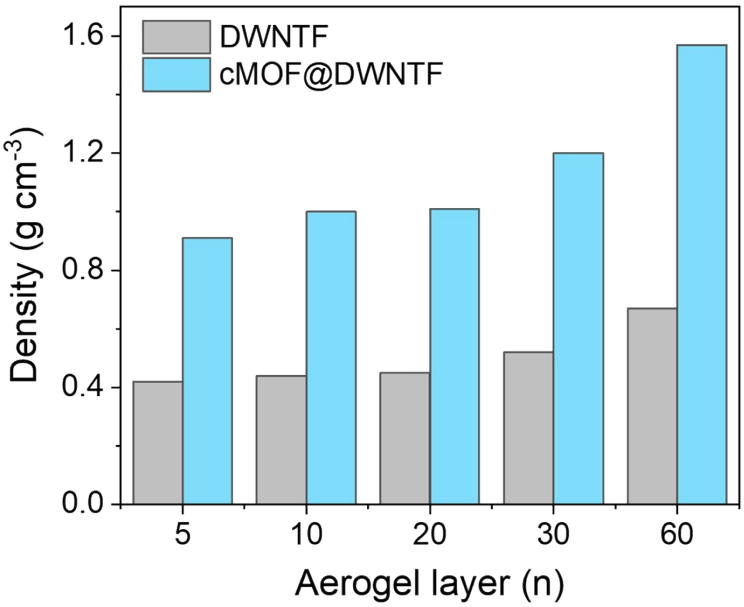

Fig. S18. Density of DWNTF and cMOF@DWNTF with different aerogel layers.

Table S1. Summary of the properties of DWNTF and cMOF@DWNTF with different aerogel layers.

	Thickness (nm)		Areal density ($\times 10^{-5}$ g cm^{-2})		Density (g cm^{-3})		Conductivity (S cm^{-1})	
	DWNTF	cMOF@ DWNTF	DWNTF	cMOF@ DWNTF	DWNTF	cMOF@ DWNTF	DWNTF	cMOF@ DWNTF
5	48	52	0.20	0.48	0.42	0.91	542.7	1124.6
10	88	92	0.39	0.92	0.44	1.00	600.8	1261.0
20	134	140	0.60	1.41	0.45	1.01	701.0	1346.0
30	223	227	1.15	2.72	0.52	1.20	842.5	1862.1
60	346	352	2.33	5.52	0.67	1.57	1724.3	3120.1

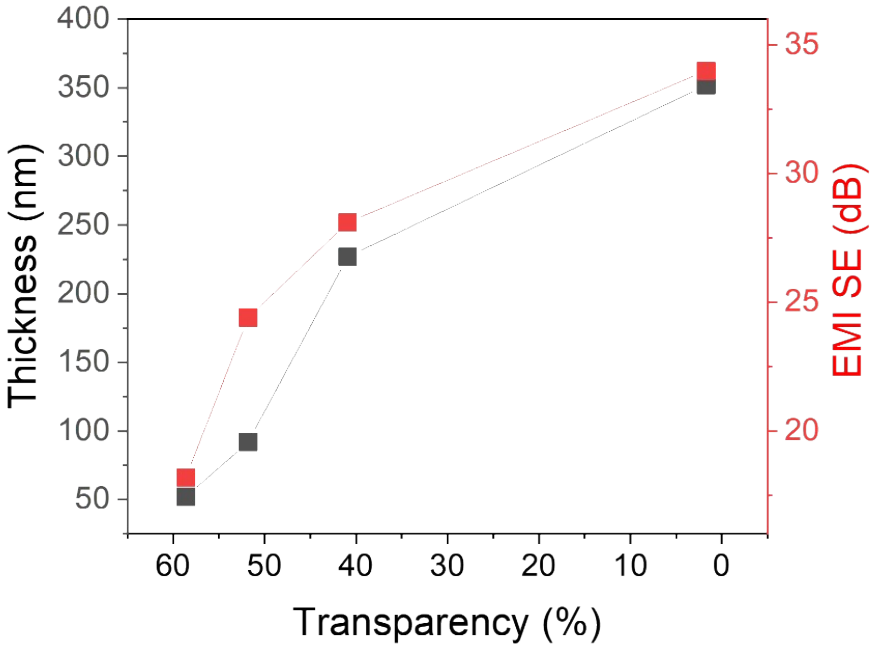

Fig. S19. Transparency versus thickness and EMI SE of cMOF@DWNTF with different aerogel layers.

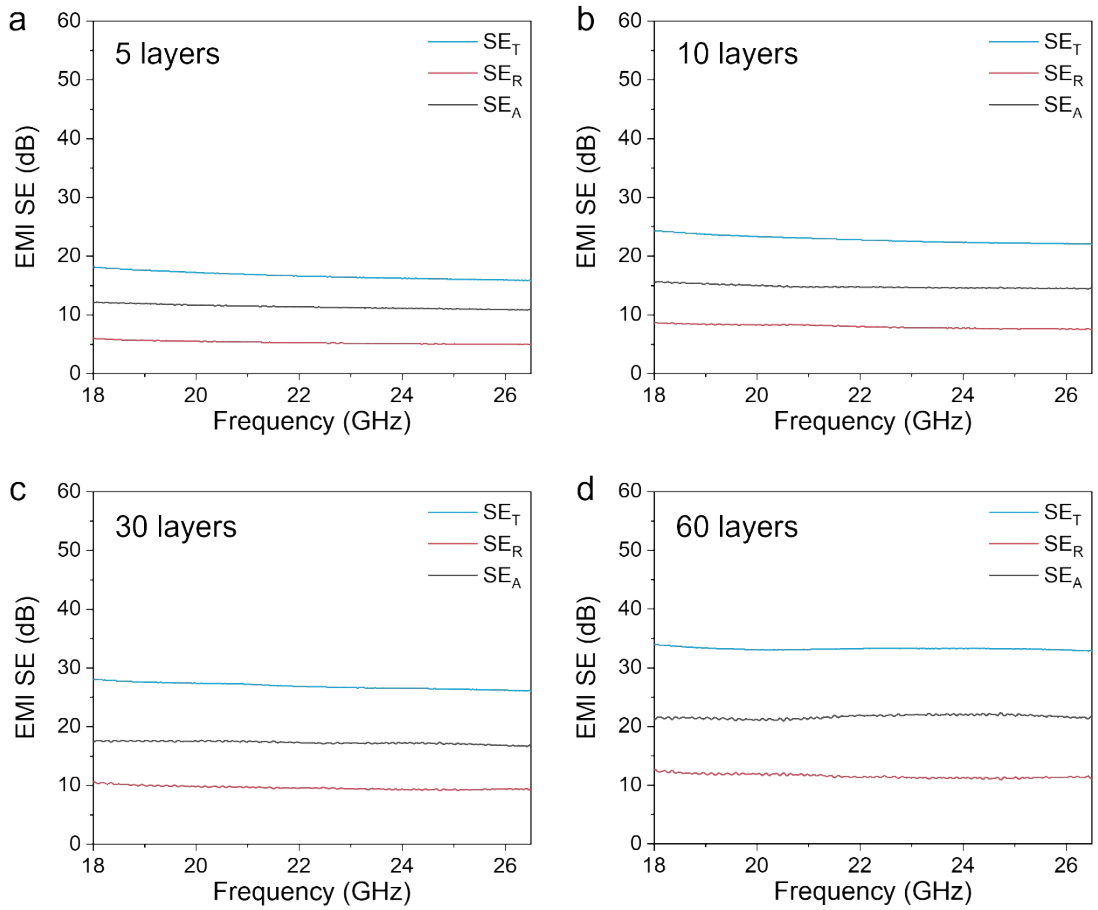

Fig. S20. EMI SE_T, SE_R, and SE_A of cMOF@DWNTF with a) five layers, b) 10 layers, c) 30 layers, and d) 60 layers.

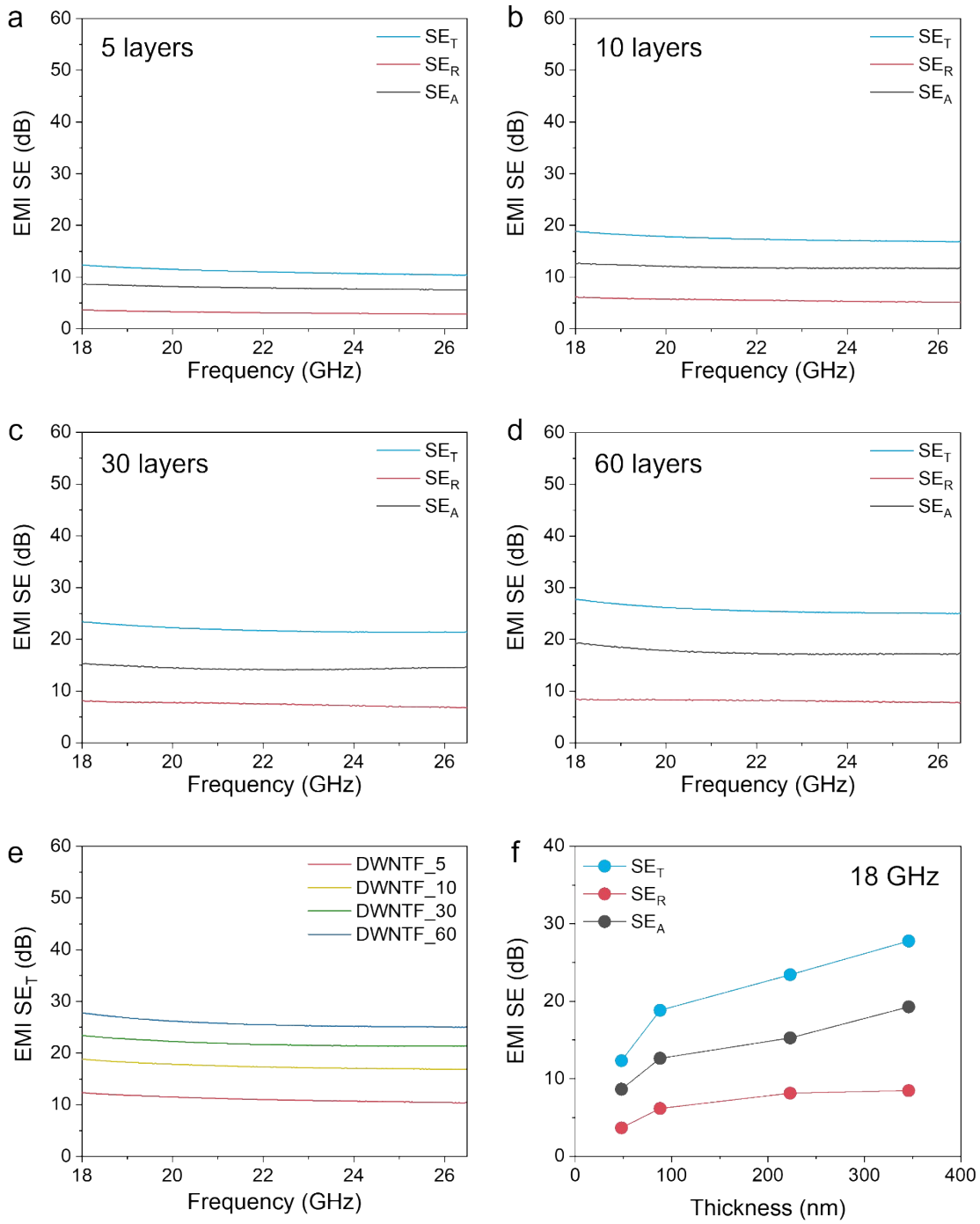

Fig. S21. EMI SE_T, SE_R, and SE_A of DWNTF with a) five layers, b) 10 layers, c) 30 layers, and d) 60 layers. e) EMI SE_T of DWNTF with different aerogel layers as a function of frequency. f) EMI SE_T, SE_R, and SE_A of DWNTF as a function of thickness.

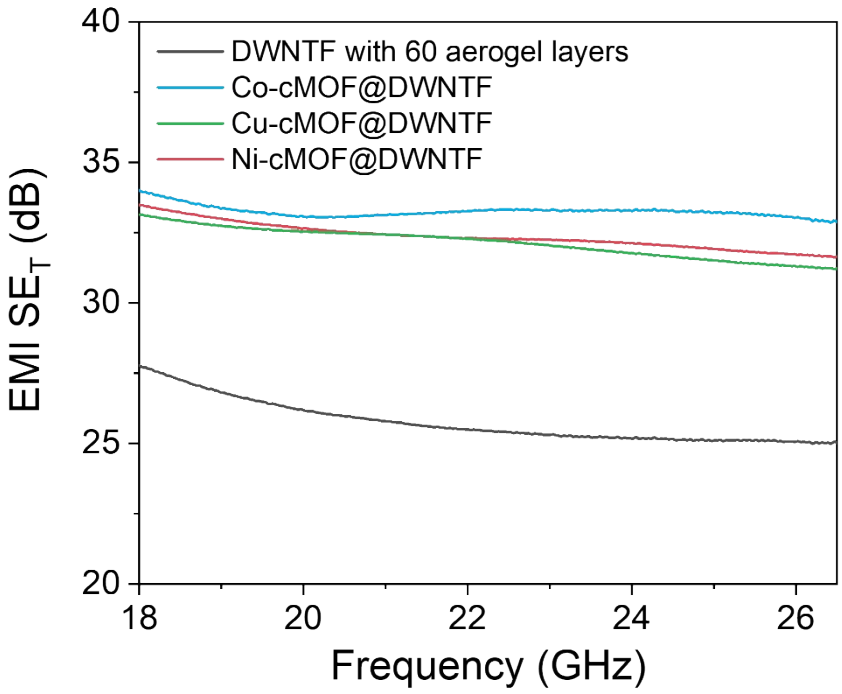

Fig. S22. EMI SE_T of Ni-, Cu-, and Co-based cMOFs@DWNTF and DWTNF with 60 aerogel layers.

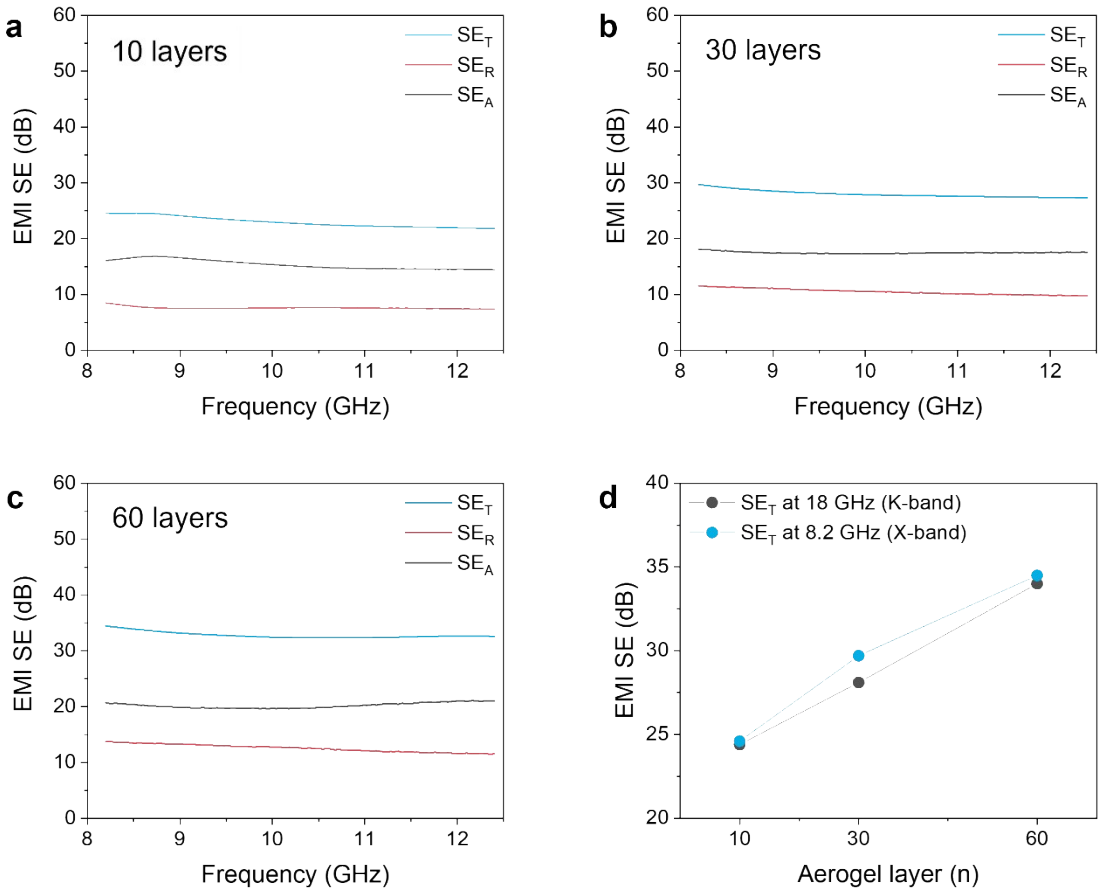

Fig. S23. EMI SE_T, SE_R, and SE_A of cMOF@DWNTF with a) 10 layers, b) 30 layers, c) 60 layers at the X-band range, and d) comparison of SE_T measured at X-band and K-band region.

Table S2. Summary of the EMI SE and specific EMI SE of the state-of-the-art EMI shielding freestanding films.

Materials		Thickness (cm)	SE (dB)	SSE/t (dB cm^2 g^{-1})	Ref.
This work	cMOF@ DWNTF (18 GHz)	5.2×10^{-6}	18.2	3.83×10^{6}	**This work**
		9.2×10^{-6}	24.4	2.66×10^{6}	
		2.27×10^{-5}	28.1	1.03×10^{6}	
		3.52×10^{-5}	34.1	6.18×10^{5}	
	cMOF@ DWNTF (8.2 GHz)	9.2×10^{-6}	24.6	2.67×10^{6}	
		2.27×10^{-5}	29.7	1.09×10^{6}	
		3.52×10^{-5}	34.5	6.18×10^{5}	
	DWNTF (18 GHz)	4.8×10^{-6}	12.3	6.17×10^{6}	
		8.8×10^{-6}	18.8	4.83×10^{6}	
		1.34×10^{-5}	23.4	2.04×10^{6}	
		346×10^{-5}	27.8	1.19×10^{6}	
MXene	Mxene foam	6.0×10^{-4}	32	1.37×10^{5}	[42]
		1.8×10^{-3}	50	6.94×10^{4}	
		6.0×10^{-3}	70	5.30×10^{4}	
	Mxene/Cellulose nanofiber paper	4.7×10^{-3}	24	2.65×10^{3}	[15]
		7.4×10^{-3}	26	2.15×10^{3}	
		1.67×10^{-2}	25	1.33×10^{3}	
	TiO_2-Mxene/Graphene film	5.25×10^{-4}	18	3.03×10^{4}	[43]

		5.59×10^{-4}	23.3	2.58×10^{4}	
		7.82×10^{-4}	23.4	1.94×10^{4}	
		9.17×10^{-4}	27	1.55×10^{4}	
	Mxene film	2.5×10^{-4}	50	8.37×10^{4}	[1]
		1.1×10^{-3}	68	2.59×10^{4}	
		4.5×10^{-3}	92	8.56×10^{4}	
		8.0×10^{-4}	57	3.08×10^{4}	
	Mxene/CNT film	2.07×10^{-5}	3.4	4.99×10^{4}	[44]
		1.7×10^{-5}	2.8	5.82×10^{4}	
	Blade-coated Mxene film	9.4×10^{-5}	46.1	1.20×10^{5}	[45]
	Mxene@CNT paper	1.0×10^{-2}	60.5	1.31×10^{4}	[46]
		4.5×10^{-3}	43.3	1.91×10^{4}	
		1.5×10^{-3}	37.2	4.16×10^{4}	
		5.0×10^{-4}	23.1	5.69×10^{4}	
	MXene/Aramid nanofiber paper	3.7×10^{-3}	48	1.32×10^{4}	[47]
		4.0×10^{-3}	36.6	1.00×10^{4}	
		3.1×10^{-3}	24.5	8.01×10^{3}	
	Sequentially bridged Mxene film	3.0×10^{-4}	56.4	6.25×10^{4}	[17]
	MXene film	3.26×10^{-4}	55.7	4.88×10^{4}	[48]
Metal	Ag@C sponge	0.3	70.1	6.12×10^{4}	[49]
		0.2	51.2	6.70×10^{4}	

		0.1	37.9	9.92×10^{4}	
	Ag nanowire/ Polyurethane nanocomposite	0.23	64	6.18×10^{3}	[50]
		0.23	50.1	7.26×10^{3}	
		0.23	20	1.09×10^{4}	
	Al foil	8.0×10^{-4}	66	3.06×10^{4}	[1]
	Cu foil	1.0×10^{-3}	70	7.81×10^{3}	[1]
	GO/Ag nanowire film	8.0×10^{-4}	62	7.75×10^{4}	[51]
Carbon	Graphene/CNT foam	0.16	38	4.00×10^{4}	[52]
	A-CNT/Polyaniline film	5.0×10^{-4}	50.2	7.49×10^{4}	[53]
	MWCNT/ Polyurethane film	0.1	21.1	5.41×10^{3}	[54]
	MCMB-MWCNT paper	1.5×10^{-2}	31	7.94×10^{3}	[55]
		6.0×10^{-2}	56	3.59×10^{3}	
	CNT sponge	0.18	54.8	3.04×10^{4}	[56]
	Carbon foam	0.2	51.2	1.71×10^{3}	[57]
	Polyurethane/rGO foam	0.25	23	1.01×10^{3}	[58]
	rGO foam/Conductive polymer	0.15	69.1	2.08×10^{4}	[59]
	Graphene foam	3.5×10^{-3}	17.3	1.01×10^{5}	[60]
		1.5×10^{-2}	50.9	7.54×10^{4}	
		3.0×10^{-2}	83	6.16×10^{4}	

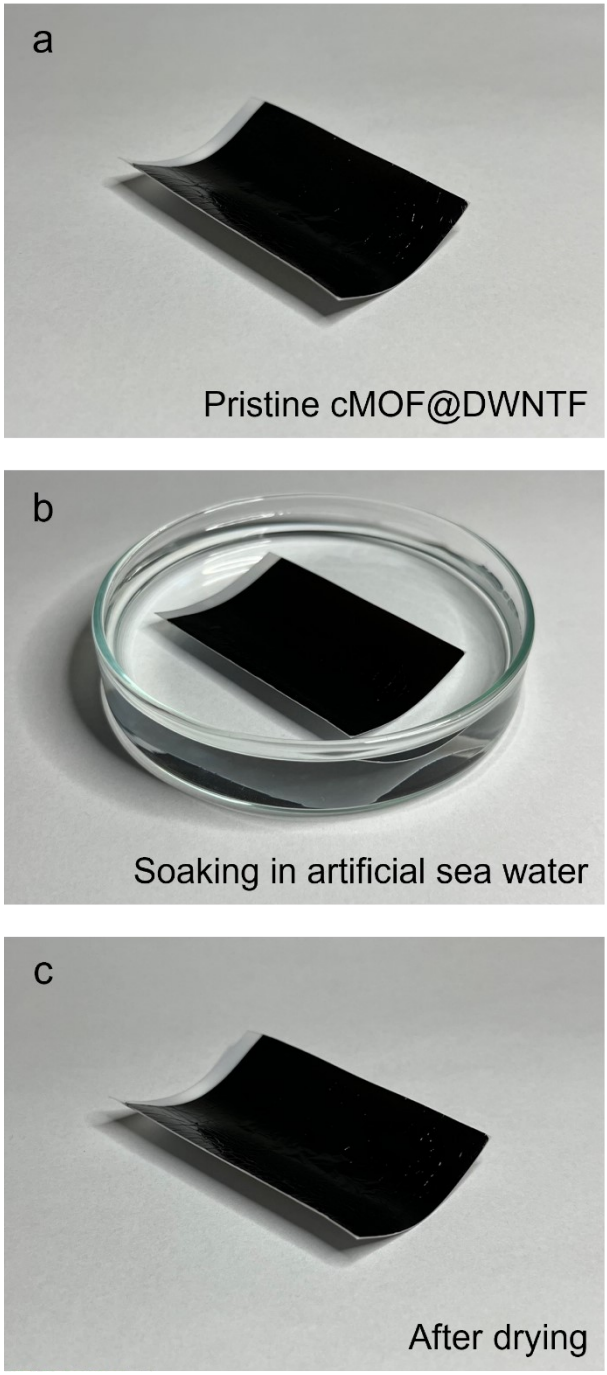

Fig. S24. Digital image of cMOF@DWNTF a) before, b) after soaking in the artificial sea water, and c) after subsequent drying. Soaking of cMOF@DWNTF was carried out while placing it on a flat PTFE substrate to uniformly wet the entire region of the film.

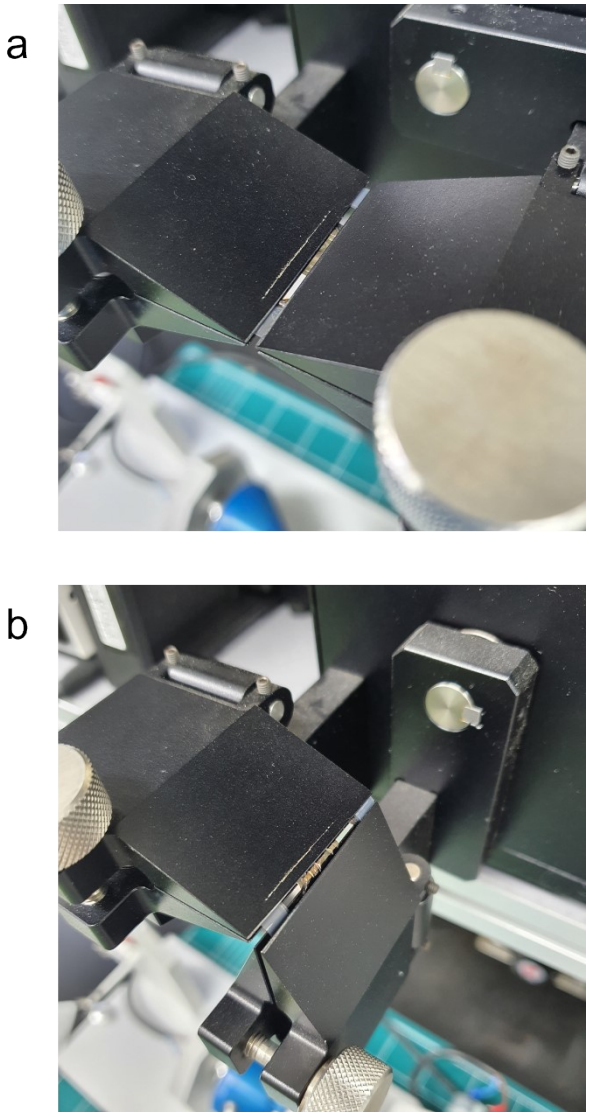

Fig. S25. Photographs of a) before and b) after bending during repeated bending tests.

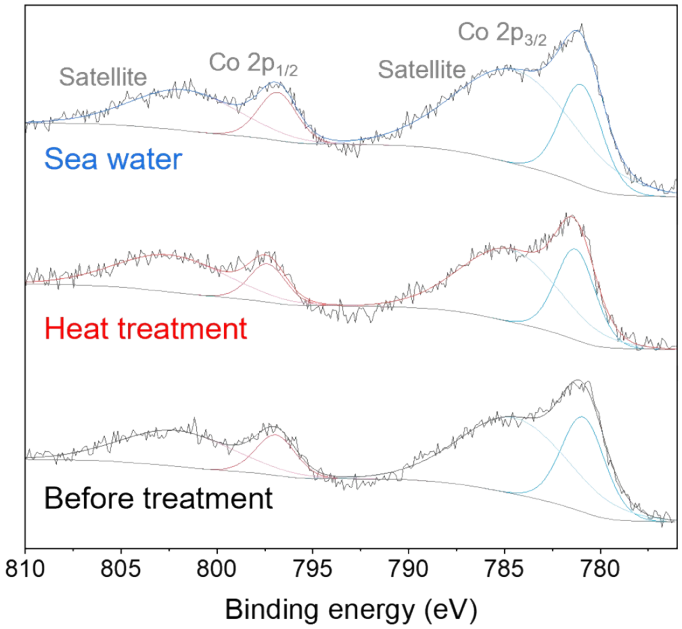

Fig. S26. XPS Co 2p spectra of cMOF@DWNTF before treatment, after heat treatment, and after soaking in sea water.

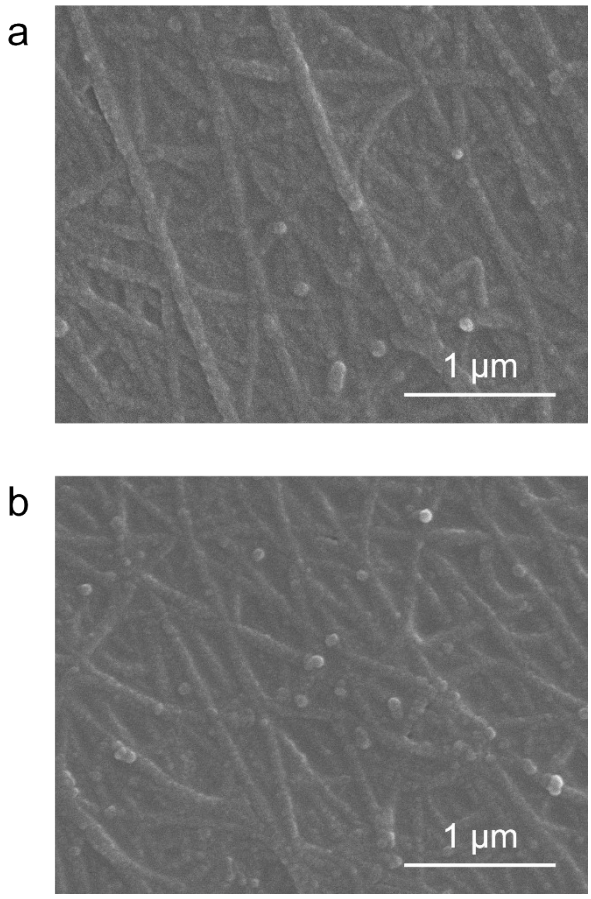

Fig. S27. SEM images of cMOF@DWNTF a) after heat treatment, and b) after soaking in sea water.

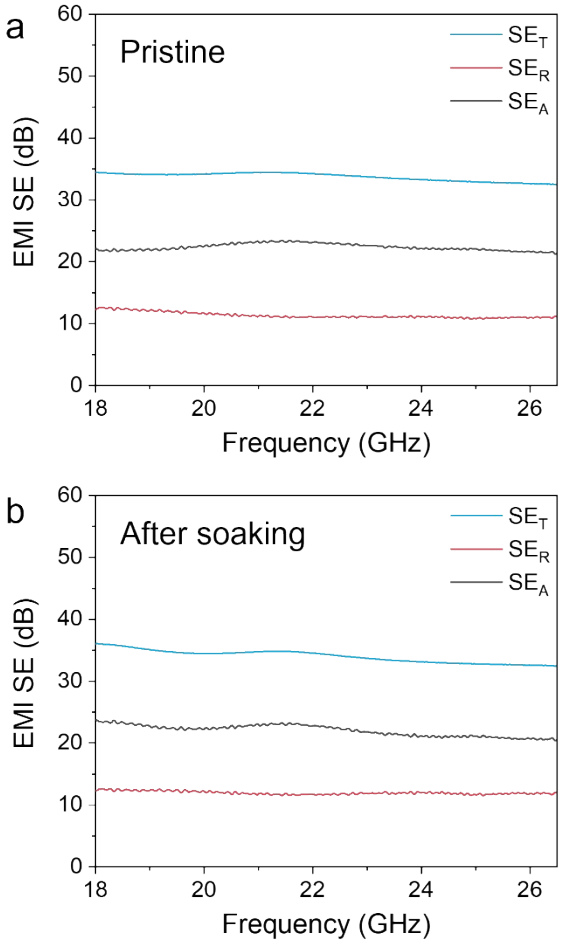

Fig. S28. EMI SE_T, SE_R, and SE_A of cMOF@DWNTF with 60 layers a) before and b) after soaking in the artificial sea water.

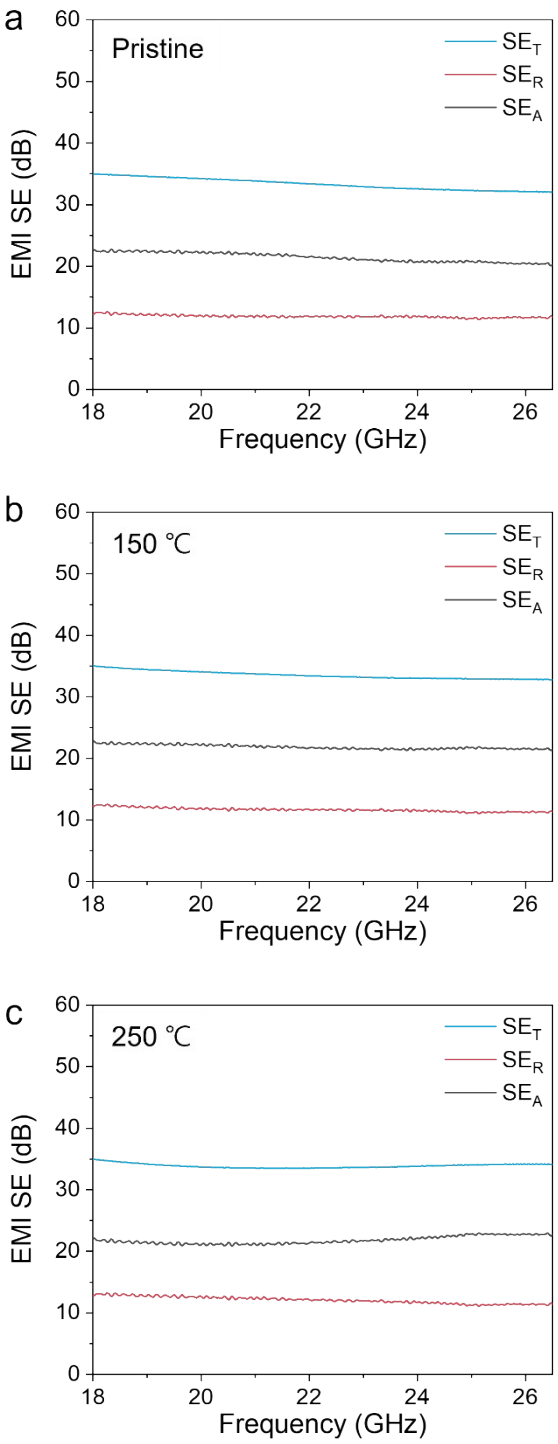

Fig. S29. EMI SE_T, SE_R, and SE_A of a) pristine cMOF@DWNTF with 60 layers and after heat treatment at b) 150 and c) 250 ℃ for 12 hours.

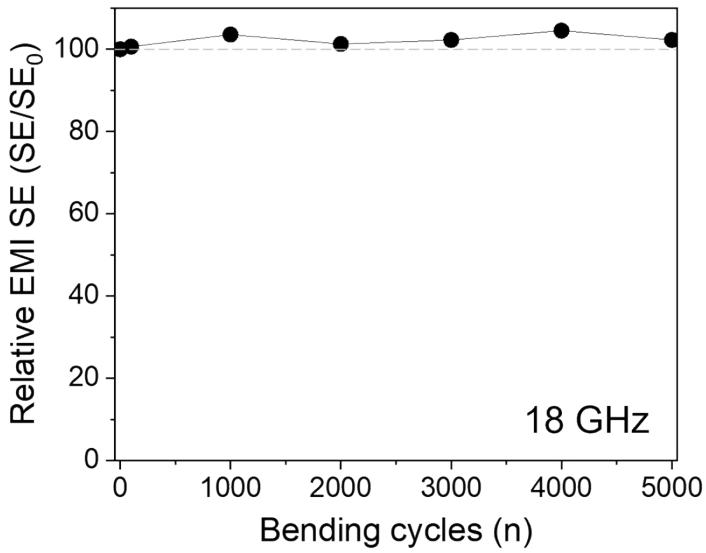

Fig. S30. Relative EMI SE of cMOF@DWNTF with 60 layers under cumulative bending test.

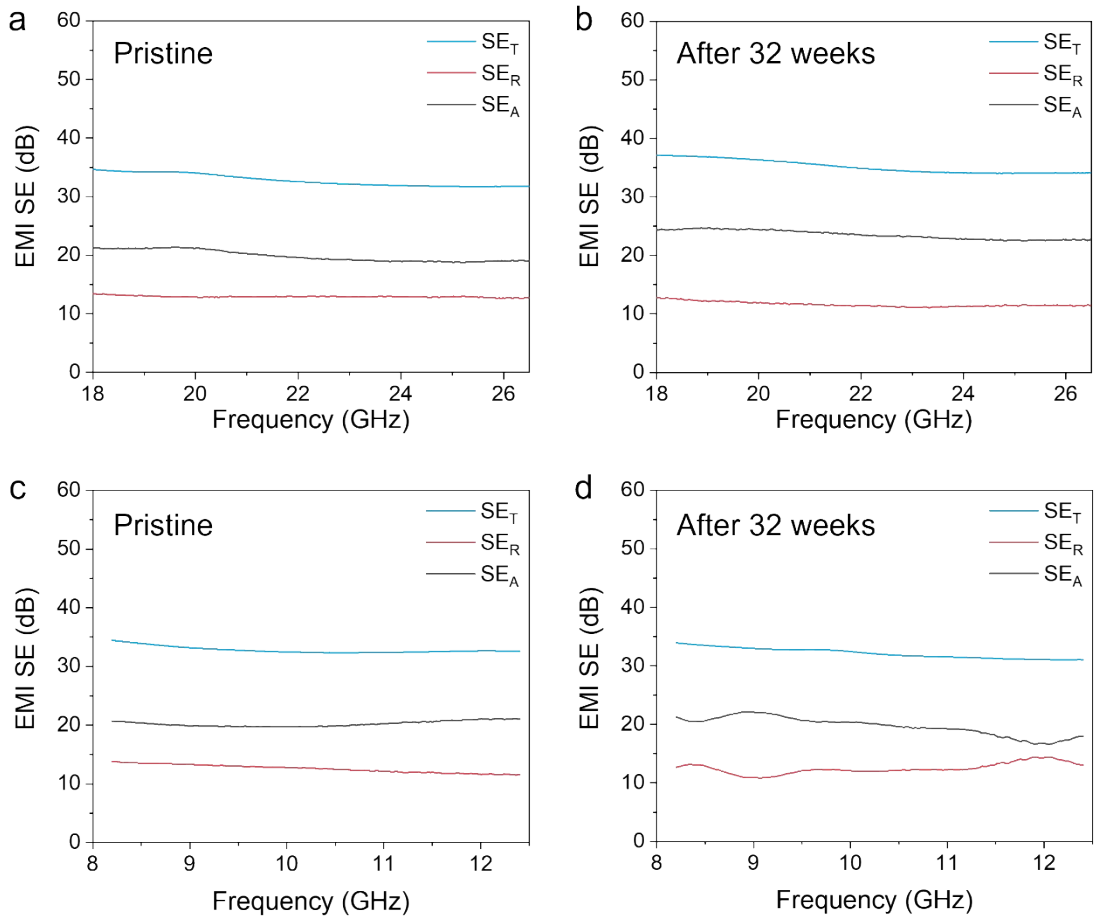

Fig. S31. EMI SE_T, SE_R, and SE_A of cMOF@DWNTF with 60 layers for 32 weeks measured at a) and b) K- and c) and d) X-band range.

Table S3. Weight record of DWNTF and cMOF@DWNTF with different aerogel layers to estimate areal density.

# of aerogel layers	DWNTF (× 10^{-4}g)										Avg. Weight (× 10^{-4}g)	Areal Density (× 10^{-5}g cm^{-2})
	#1	#2	#3	#4	#5	#6	#7	#8	#9	#10		
5	1.2	1.3	1.2	1.1	1.2	1.2	1.2	1.2	1.1	1.2	1.19	0.20
10	2.4	2.2	2.3	2.3	2.4	2.3	2.5	2.4	2.3	2.3	2.34	0.39
20	3.5	3.7	3.6	3.5	3.6	3.7	3.7	3.6	3.5	3.6	3.60	0.60
30	7.0	6.9	6.8	6.8	7.0	6.9	6.8	6.9	6.9	6.9	6.89	1.15
60	14.0	13.9	14.1	13.9	13.9	13.9	14.0	14.0	14.1	14.0	14.0	2.33
# of aerogel layers	cMOF@DWNTF (× 10^{-4}g)										Avg. Weight (× 10^{-4}g)	Areal Density (× 10^{-5}g cm^{-2})
	#1	#2	#3	#4	#5	#6	#7	#8	#9	#10		
5	2.8	2.9	3.0	2.9	2.8	2.8	2.9	2.9	2.8	3.0	2.88	0.48
10	5.5	5.5	5.6	5.4	5.5	5.5	5.6	5.6	5.5	5.5	5.52	0.92
20	8.6	8.4	8.4	8.6	8.4	8.4	8.5	8.5	8.4	8.4	8.46	1.41
30	16.4	16.3	16.3	16.4	16.3	16.4	16.3	16.3	16.3	16.2	16.3	2.72
60	33.1	33.1	33.1	33.2	33.1	33.1	33.2	33.1	33.1	33.1	33.1	5.52

References

42. J. Liu, H. B. Zhang, R. Sun, Y. Liu, Z. Liu, A. Zhou and Z. Z. Yu, *Adv. Mater.*, 2017, **29**, 1702367.

43. C. Xiang, R. Guo, S. Lin, S. Jiang, J. Lan, C. Wang, C. Cui, H. Xiao and Y. Zhang, *Chem. Eng. J.*, 2019, **360**, 1158-1166.

44. G. M. Weng, J. Li, M. Alhabeb, C. Karpovich, H. Wang, J. Lipton, K. Maleski, J. Kong, E. Shaulsky and M. Elimelech, *Adv. Funct. Mater.*, 2018, **28**, 1803360.

45. J. Zhang, N. Kong, S. Uzun, A. Levitt, S. Seyedin, P. A. Lynch, S. Qin, M. Han, W. Yang and J. Liu, *Adv. Mater.*, 2020, **32**, 2001093.

46. J. Wang, X. Ma, J. Zhou, F. Du and C. Teng, *ACS nano*, 2022, **16**, 6700-6711.

47. R. Yang, X. Gui, L. Yao, Q. Hu, L. Yang, H. Zhang, Y. Yao, H. Mei and Z. Tang, *Nano-Micro Lett.*, 2021, **13**, 66.

48. J. Lipton, J. A. Röhr, V. Dang, A. Goad K. Maleski, F. Lavini, M. Han, E. H. R. Tsai, G.-M. Weng, J. Kong, E. Riedo, Y. Gogotsi and A. D. Taylor, *Matter*, 2020, **3**, 546-557.

49. Y. J. Wan, P. L. Zhu, S. H. Yu, R. Sun, C. P. Wong and W. H. Liao, *Small*, 2018, **14**, 1800534.

50. Z. Zeng, M. Chen, Y. Pei, S. I. Seyed Shahabadi, B. Che, P. Wang and X. Lu, *ACS Appl. Mater. Interfaces*, 2017, **9**, 32211-32219.

51. H. Jia, X. Yang, Q.-Q. Kong, L.-J. Xie, Q.-G. Guo, G. Song, L.-L. Liang, J.-P. Chen, Y. Li and C.-M. Chen, *J. Mater. Chem. A*, 2021, **9**, 1180-1191.

52. Q. Song, F. Ye, X. Yin, W. Li, H. Li, Y. Liu, K. Li, K. Xie, X. Li and Q. Fu, *Adv. Mater.*, 2017, **29**, 1701583.

53. H. Li, X. Lu, D. Yuan, J. Sun, F. Erden, F. Wang and C. He, *J. Mater. Chem. C*, 2017, **5**, 8694-8698.

54. Z. Zeng, H. Jin, M. Chen, W. Li, L. Zhou and Z. Zhang, *Adv. Funct. Mater.*, 2016, **26**, 303-

310.

55. A. Chaudhary, S. Kumari, R. Kumar, S. Teotia, B. P. Singh, A. P. Singh, S. Dhawan and S. R. Dhakate, *ACS Appl. Mater. Interfaces*, 2016, **8**, 10600-10608.

56. D. Lu, Z. Mo, B. Liang, L. Yang, Z. He, H. Zhu, Z. Tang and X. Gui, *Carbon*, 2018, **133**, 457-463.

57. L. Zhang, M. Liu, S. Roy, E. K. Chu, K. Y. See and X. Hu, *ACS Appl. Mater. Interfaces*, 2016, **8**, 7422-7430.

58. J. N. Gavgani, H. Adelnia, D. Zaarei and M. M. Gudarzi, *RSC Adv.*, 2016, **6**, 27517-27527.

59. Y. Wu, Z. Wang, X. Liu, X. Shen, Q. Zheng, Q. Xue and J.-K. Kim, *Appl. Mater. Interfaces*, 2017, **9**, 9059-9069.

60. H. Kashani, M. Giroux, I. Johnson, J. Han, C. Wang and M. Chen, *Matter*, 2019, **1**, 1077-1087.